MICRO-PRECISION INTERFEROMETER: POINTING CONTROL SYSTEM

John F. O'Brien and Gregory W. Neat
Jet Propulsion Laboratory, California Institute of '1'ethnology, Pasadena, CA

ABSTRACT

This paper describes the development of the wavefront tilt (pointing) control system for the JPL Micro-Precision Interferometer (MPI). This control system employs piezoelectric actuators and a digital imaging sensor with feedback compensation to reject errors in instrument pointing. Stringent performance goals require large feedback, however, several characteristics of the plant tend to restrict the available bandwidth. A robust 7th-order wavefront tilt control system was successfully implemented on the MPI instrument, providing sufficient disturbance rejection performance to satisfy the established interference fringe visibility requirement.

1. INTRODUCTION

Next generation astrophysics missions will require measurement accuracies which are a factor of 10 better than existing full aperture systems, such as the Hubble Space Telescope (HST). Interferometry offers a new means of extending the effective telescope aperture and thus achieving the desired measurement accuracies without requiring a full aperture system. Onc concept for a future space-based interferometer is the Orbiting Stellar Interferometer (0S1), shown in Figure 1 [I].

0S1 is a mission concept for a first-generation space interferometer with astrometric and imaging goals, The approach uses three collinear Michelson interferometers, each defined by a pair of collecting apertures or siderostats, to perform parcscc-level astrometric measurements and milliarcscc-level imaging of the heavens. Rather than depend on accurate base body pointing of the entire spacecraft as with full aperture systems (e.g., HST) this design utilizes high bandwidth optical sensing (metrology systems) and high bandwidth control of optical elements to achieve precision pointing requirements.

Figure 2 shows a schematic diagram of a single Michelson interferometer observing a stellar sour. The active optical layer contributes significantly to the bottom-line vibration attenuation challenge: stabilize and measure the stellar fringe position down to the 10-nanometer (RMS) level. Fringe stabilization to this level implies the light path from the star, through one arm of the interferometer (S,1 ,2,3,4,5,6,7,8,9 in Figure 2) equals the light path from the star, through the other arm of the interferometer (S,1',2',3',4',5',6',7',8',9',9 in Figure 2). Stabilization of the resulting interference pattern at the beam combiner (component 9 in Figure 2) requires successful operation of two optical subsystems: the pointing control subsystem and the fringe tracking subsystem. The pointing control subsystem independently points each interferometer arm at the same target star by articulating the respective siderostat (1 or 1') and fast steering mirror (4 or 4') based on the two stellar images from (he pointing camera. Once each interferometer arm is "looking" at the same star, the fringe detector can measure stellar fringe position. The fringe tracking subsystem stabilizes the fringe position in the presence of spacecraft disturbances and rigid body motion. The fringe tracker subsystem has a single actuator in one of the interferometer arms which is the high bandwidth, high dynamic range active delay line (5, 6, 7 in Figure *2).* This actuator translates linearly, introducing an optical path delay, as commanded by the fringe detector, in order to equalize the two optical paths. This paper focuses on the pointing control system.

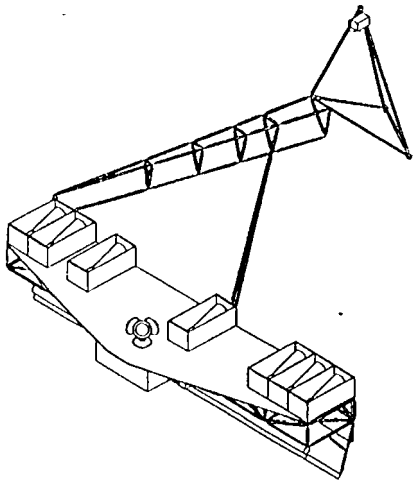

Figure 1. Orbiting Stellar Interferometer.

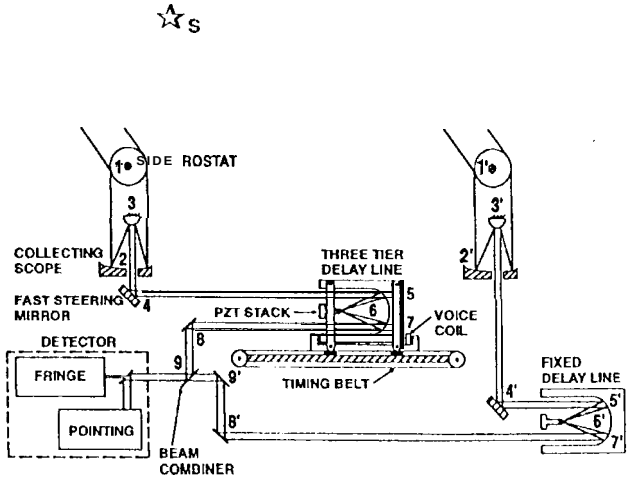

Figure 2. Stellar optical path for a Michelson interferometer.

Each of the three colinear 0S1 interferometers stabilizes the stellar fringes of a specific star. Two interferometers (guide interferometers) stabilize the fringes of bright target stars [1]. These interferometers provide a high bandwidth, parcscc-level measurement of tbc attitude of the instrument's colinear baselines.- The bright target stars provide ample signal level for the guide interferometer pathlength and pointing control subsystems. The third interferometer (science interferometer) observes the dim science object. This paper addresses the pointing control system for a bright star interferometer.

2. JPL MICRO-PRECISION INTERFEROMETER

Tbc Micro-Precision Interferometer (MPI) is a ground-based testbed that is dimensionally a full-scale model of 0S1. The testbed contains all necessary systems to perform a space-based astrometric measurement. For a complete description of the MPI instrument, the reader is directed to reference 2.

Figure 3 traces the stellar optical path through the star simulator and testbed optical train. Tbc inset in Figure 3 indicates the changes in the stellar beam cross section at the respective locations along the optical path. The following discussion traces the stellar optical path through the system. For further details on the optical system, see reference 3.

The "star" source is the laser head of a commercial laser interferometer system that sits on a pneumatically suspended optical table. The source feeds polarization specific beams into each of the MPI siderostats. The two interferometer beam paths experience symmetrical reflections in the two interferometer arms on the testbed. The following traces the "inboard" beam path (collecting aperture on the right-hand side of the Figure) without loss of generality. The two-axis gimbaled siderostat mirror contains a 12-mm-diameter retroreflector used by the internal metrology system. Therefore, the beam leaving the siderostat consists of an annular stellar beam and a central infrared metrology beam. A 90/10 beam splitter picks off 10% of this beam and sends it to

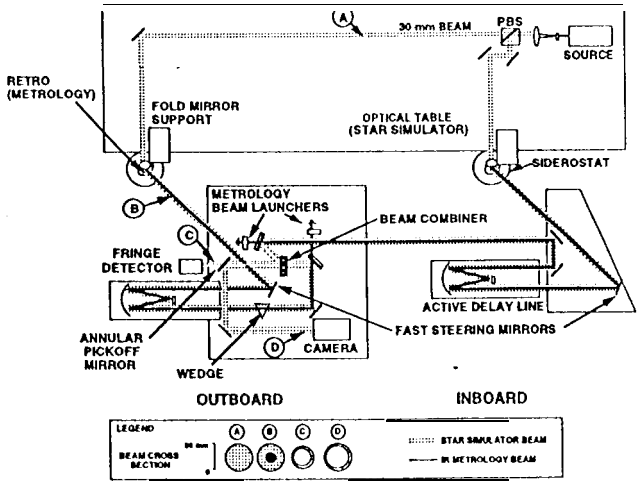

Figure 3. *Optical layout of the first MPI baseline from star simulator to optical detectors. The inset shows the beam cross section at different points in the optical path.*

atom-se acquisition sensor, used by the siderostat to initially acquire the star. The remaining light travels to the 2-axis, high bandwidth fast steering mirror which sends the light into the active delay linc.

The output beam from the active delay linc reflects off three fold mirrors, sending the beam to the "outboard" plate (closest to the collecting aperture on the left-hand side). The third fold mirror directs the beam to the beam combiner where the beam from the inboard siderostat is reflected to join the transmitted beam from the outboard siderostat. After the beam combiner, the central region of the combined stellar beams passes through the hole in the annular pickoff mirror to a fringe detector as a single beam with two orthogonal components with frequencies that differ by 1.8 MHz and phase that depends on the optical path of each. The detector, a standard receiver for tbc commercial interferometer, produces a 1.8-MHz heterodyne signal with a phase that varies as the (optical pathlength difference) (OPD) of the stellar beams changes. The annular pick-off mirror reflects the outer region (30-mm OD and 25-mm ID) of each stellar beam and directs them to a telescope with a focal length of 423 mm. The telescope focuses the stellar beams onto a CCD camera.

Finally, the outboard optical path contains an additional 1-arc-minute annular wedge that contains a central hole that corresponds to the pick-off mirror hole diameter. This causes the outer annular region of the beam from the outboard siderostat to be offset by 1 arc minute while the center portion passes through undeviated. Thus, at the pick-off mirror, the central portions of the two beams are parallel while the outer regions diverge at an angle of 1 arc minute. The two reflected annuli arc brought to a focus on the CCD camera by a telescope. The wedge, therefore, enables a simple means to sense wave tilt error in the optical system with a single sensor.

3. MPI POINTING CONTROL SYSTEM

The purpose of the pointing control subsystem is to ensure that each arm of the interferometer points at the same target star. Equivalently, this subsystem guarantees the wave fronts from the two collecting apertures are parallel. The nominally acceptable percentage of fringe visibility loss attributed to guiding errors is 5%. From Colavita [4], this corresponds to aO. 1 ?Jd stability value. ForM PI (λ=633 nm, d=30 mm), this corresponds to 2.1 μrad, rms.

This angular stability of the stellar beams must be maintained in the presence of disturbances. For 0S1, these include errors associated with the attitude control system (ACS) deadband, and structural vibrations driven by attached sources of force. Tbe MPI disturbance environment will additionally include rigid body swaying of the instrument structure on its suspension system, and motion of the pseudo-star optical table due to laboratory floor vibrations. The disturbance rejection task of the MPI wavefront tilt control system is somewhat more challenging than that of its peer on 0S1, in that the 0S1 structure will not sway, and its target stars will not shake.

Since each arm of the interferometer must independently "point", each arm has a stand alone pointing control subsystem. This subsystem has two actuators: the low-bandwidth, Iargc-angle siderostat; and the high-bandwidth, precise, fast steering mirror. As in the case of the eventual 0S1 mission, the main function of the MP1 siderostat is to acquire the star. Once acquired, the siderostat is locked down during the observation period. Therefore, the fast steering mirrors arc the pointing control subsystem disturbance rejection actuators. The MPI high voltage fast steering mirror has a bandwidth of 1 kHz and an angular range of ±35arcsecs. Three symmetrically orientated piezo actuators position the mirror.

The sensor for the pointing control subsystem is a high-frame-rate 32x 32 pixel CCD camera. The camera screen is divided in half so that each arm of the interferometer has an assigned region on the camera to be imaged. This is possible duc to the annular wedge discussed in Figure 3. During closed loop operation, only a 5 x 5 pixel window is transferred from the camera to the processor enabling high sample rates. The dedicated processor for this loop calculates x, y centroid values for this 5 x 5.

4. CONTROL DESIGN

The "fundamental" approach to the wavefront tilt control design involves reducing the problem to two independent S1S0 control systems pcr FSM (x-axis tilt and y-axis tilt). To facilitate this, the three piezo translation commands must bc transformed into two orthogonal tilts. This is achieved through the use of an analog tilt decoupling circuit. The effectiveness of the tilt decoupler must bc verified experimentally in the plant identification process before the compensator design begins.

4.1 Plant Identification

l'here arc three primary characteristics of the wavefront control problem that must bc quantified through plant identification: cross-axis coupling, plant equivalence, and plant behavior.

4.1.1 Cross-Axis Coupling: With the tilt decoupling circuit in place, the fsm's arc two dcgrcc-of-freedom actuators. Thus, there arc two plants associated with each fsm (x-axis tilt, and y-axis tilt). If there is no cross-axis coupling between x and y rotations (indicating the effectiveness of the analog decoupling circuits, and the proper angular orientation of the fsm's and the CCD), then the control problem involves the design of two decoupled S1S0 compensators pcr fsm. This would bc a far more straightforward problem than the design of a coupled controller that would be required if significant cross coupling was present.

Figure 4 compares two frequency response functions (FRF). The coherent FRF is a measurement of inboard spot motion in the x direction on the CCD due to inboard fsrn mirror rotation in the same direction. The incoherent transfer function is the same measurement except the output is inboard spot motion in they-direction (the "off axis"). This comparison seems to indicate the lack of cross coupling between fsm tilts (except in the neighborhood of 300 Hz). This condition is the same with the outboard fsm. Thus, the control problem consists of four indcpcndcnt and decoupled plants, allowing the implementation of four *separate S1S0* compensators (the "fundamental" approach).

4.1.2 Plant Equivalence: Figure 5 compares the four plant transfer function moduli for the wavefront tilt control problem. All four plant FRFs have very similar shapes, and arc within a fcw dB of each other in magnitude. This allows the implementation of four *separate* and *identical S1S0* compensators. The block diagram for one of these control loops is shown in figure 6.

4.1.3 Plant Behavior: Figure 7 is the modulus anti argument of the outboard y-direction plant transfer function (recall that all four plant transfer functions arc essentially identical). The plant modulus is rather friendly, being flat until approximately 250 Hz, where local dynamics of the fast steering mirror appear. These local modes were originally much higher q, and were reduced through the application of damping material to the fast steering mirror mount. The lack

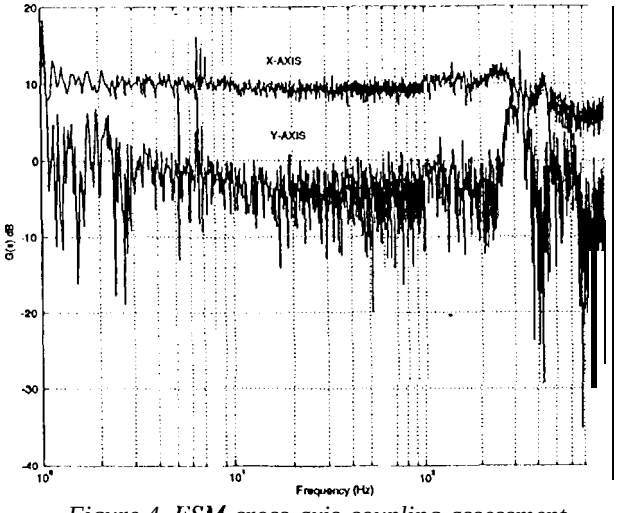

Figure 4. FSM cross-axis coupling assessment

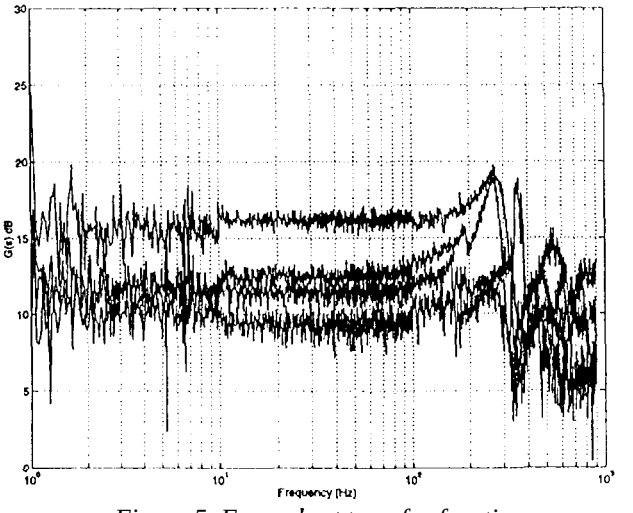

Figure 5. Four plant transfer functions

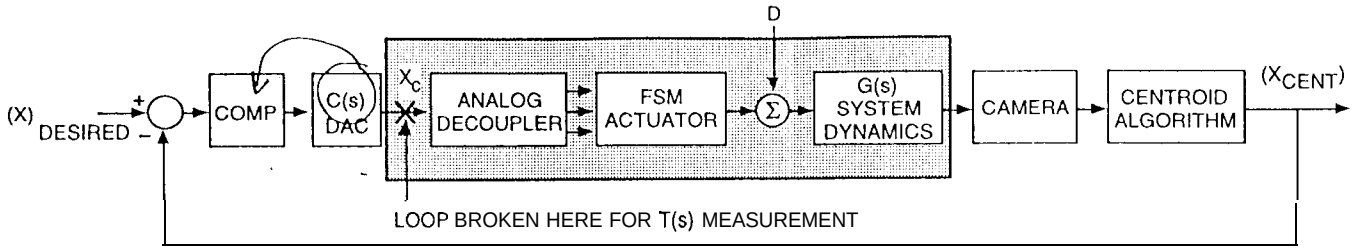

Figure 6. Block diagram of the pointing control subsystem. The shaded regions indicate the analog components.

of coupling to modes of the interferometer structure is testament to the low moments of inertia and small displacements associated with the fast steering mirror.

The argument of the plant transfer function of Figure 7 shows an approximately 700 μs time delay in the measurement. This time delay is due to integration time, centroid calculation, digital-to-analog conversion of the error signal, and other effects. These effects cannot be altered, and the time delay must be considered "plant delay".

4,2 Feedback limitations

Disturbance rejection is the goal for this control system, thus maximum feedback should be obtained. For this, the crossover frequency of the control system should be as high as plausible. There are four major aspects of this control problem, however, that tend to reduce the allowable bandwidth.

1. From communication with Colavita, it is established that even for the guide interferometers of 0S1, whose stellar targets are purposefully bright, the photon count will be insufficient to allow for CCD measurements beyond 100 Hz. Although MPI, whose stellar target is a HcNe laser source, has copious target brightness, the design of an indiscriminately high bandwidth wavefront tilt control system would not be traceable to a flight system.
2. The plant transport lag described previously causes catastrophic phase delay in frequencies beyond 100 Hz, and essentially caps the available bandwidth to this value.
3. The fsm modes at -300 Hz provide an ancillary limit to the available feedback. Although not terribly destructive in their contribution to plant phase delay, the asymmetry of the mount modes increase off-axis coupling. This limits the bandwidth of the "fundamental" control system.
4. The small amplitude range of the fast steering mirrors makes them rather sensitive to saturation. With the siderostats locked down after acquisition, the fsm's have no source of desaturation. Thus, care should be taken to ensure that the resulting control system retains stability in the presence of a saturation non-linearity. This condition precludes the design of a Nyquist-stable control system (that is, a Nyquist-stable control system without non-linear dynamic compensation).

[1] Personal communication with Mark Colavita of JPL

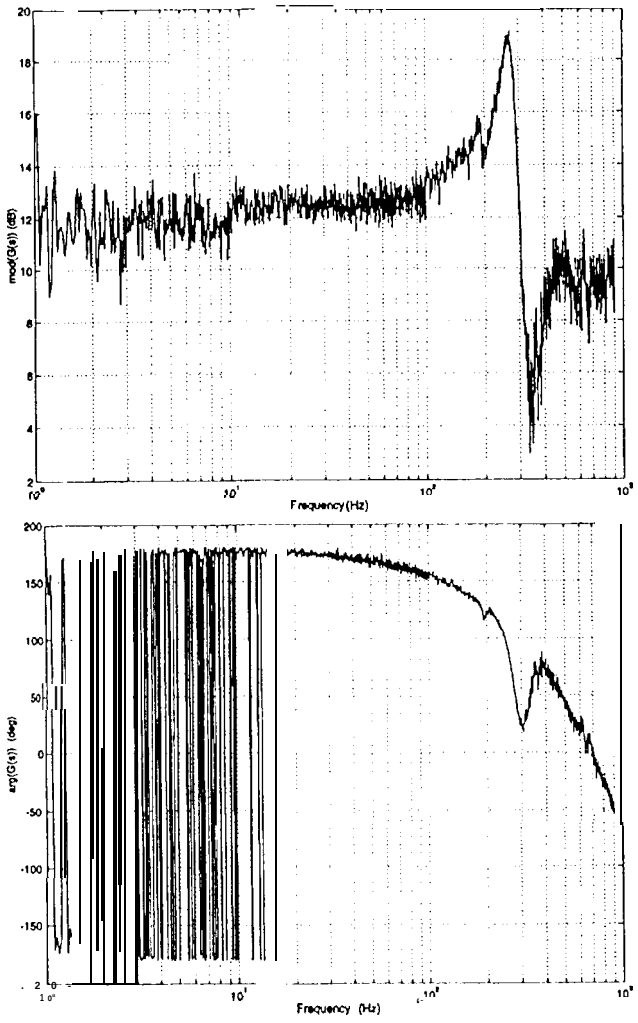

Figure 7. Outboard y-direction plant transfer function

For these reasons, the bandwidth of the wavefront control system is limited to 100 Hz by (1) and (2), and the slope of the roll-off is limited at all frequencies below the crossover by (4). These present a severe limitation to the available feedback, and thus the disturbance rejection performance of the controller. For this, the compensator should be carefully shaped to squeeze as much feedback into the available bandwidth as possible without wanton sacrifice of robustness.

In summary, the control design drivers are:

- have cross-over frequency at <100 Hz.
- maximize feedback
- retain stability in the presence of actuator saturation.

4.3 Compensator Design and Implementation

Figure 8 shows the modulus and argument of a 7th order compensator (C(s) in Figure 6) for the wavefront control system. The compensator breaks at 1 Hz to a -10dB/oct roll-off. The function "steps" at approximately 100 Hz, and then breaks again to a 3rd-order roll-off at -250 Hz. This is a rough approximation of the Bode Optimal Cut-off [5]. The step at 100 Hz provides a phase advance in the neighborhood of the crossover frequency, in this case 80 Hz. The third-order roll-off at 250 Hz was chosen to adequately gain stabilize the fsm mount modes at -300 Hz. The severe phase delay associated with this was considered secondary to the gigantic phase delay due to the plant time delay. From the Bode phase-gain relationship for minimum phase systems, the -10 dB/oct roll-off results in a phase delay of 150 deg. This provides a minimum of 30 degrees of phase margin for the control system if the loop gain is decreased by any value (saturation).

The loop transmission, T(s), of the digitally implemented wavefront control system for the inboard x direction is shown in Figure 9. The phase stability margin is 30 degrees at 80 Hz. The gain margin is 6 dB at 150 Hz. The fsm modes are well gain stabilized. The control system has at least 30 degrees of phase margin if the loop gain is decreased by any value, or increased by 3 dB. The return ratios for the other three wavefront control systems were nearly identical to Figure 9.

The compensator was discretized using a bilinear approximation, and was implemented on a Heurikon 68040 processor at a sample rate of 4 kHz. The command signal was converted to analog by a Data Translation 1403 16-bit digital-to-analog converter. This implementation adds hold and computation time delays to the already present plant time delay.

4.4 Wavefront Tilt Controller Performance

Figure 10 compares two frequency response functions measured on the MPI testbed. The solid curve shows the angular jitter of the inboard stellar beam (single axis) measured by the CCD when the structure is driven by a mini-shaker attached to its vertex with the wavefront tilt control system *open loop. The* dashed curve is the same measurement with the wavefront tilt controller operational. Figure 10 verifies the disturbance rejection potential of the control system evident in the loop gain plot of Figure 9. This result is repeatable for the other three controllers.

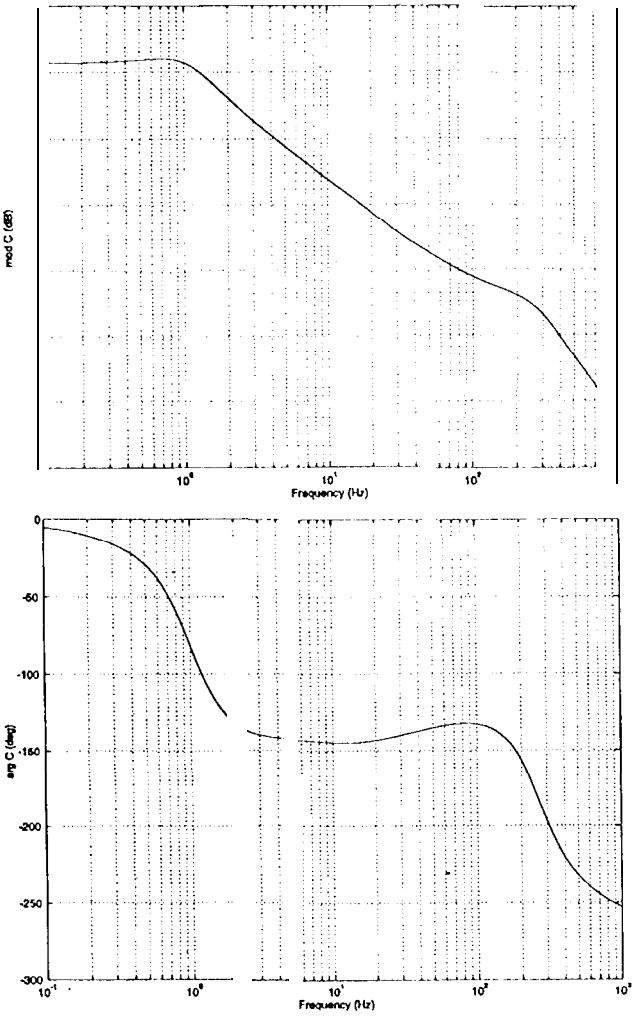

Figure 8. Modulus and argument of the MPI pointing control compensator, C(s)

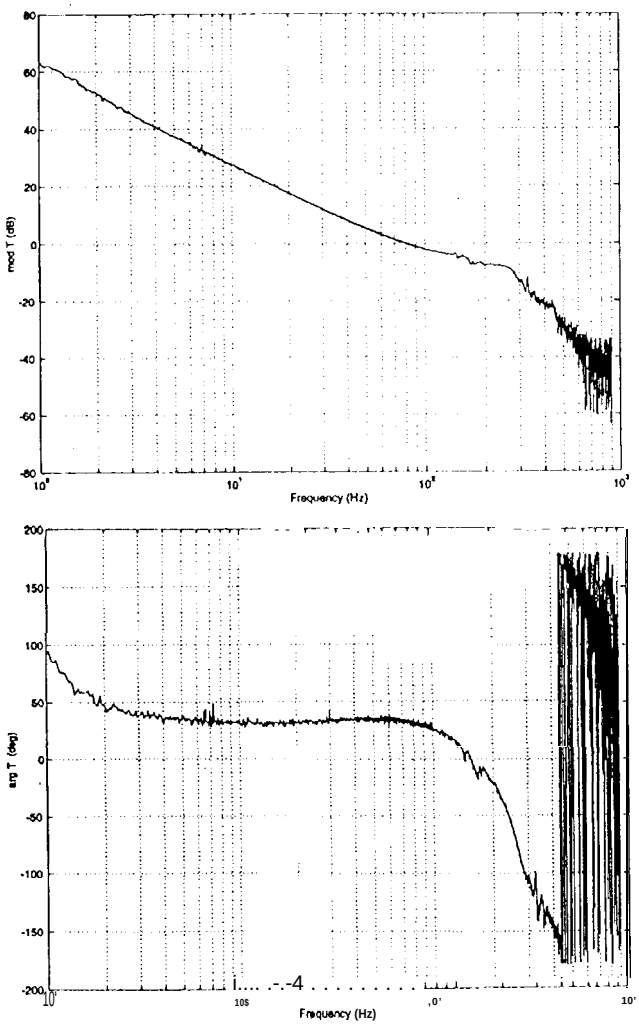

Figure 9. Modulus and argument of the MPI pointing control loop transmission, T(s)

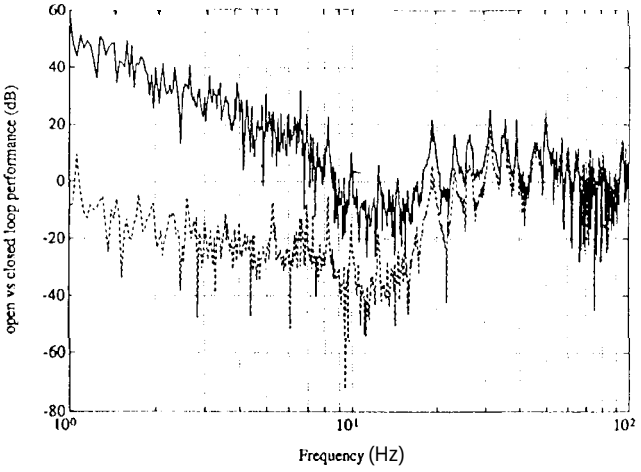

Figure 10. Pointing control performance (frequency domain assessment)

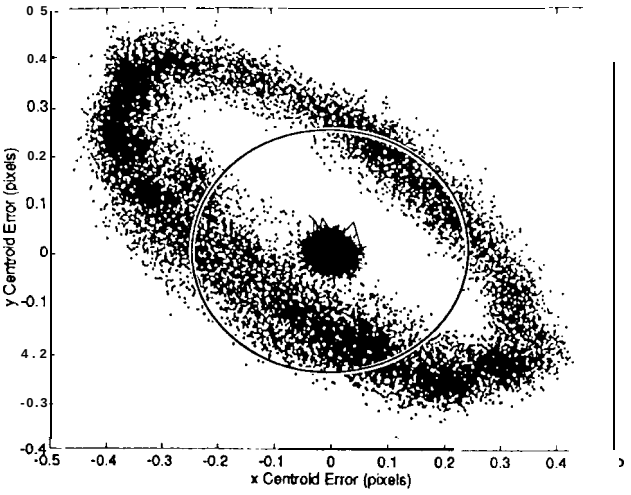

Figure 1 I. Pointing control performance (time domain asses sment)

Beyond the straightforward assessment of loop gain and margins of stability, the ability of the wavefront tilt control system to restrict fringe visibility loss due to guidance errors in the presence of disturbances should be experimentally verified. Figure 11 shows X and Y centroid errors for onc stellar spot, plotted against each other in open (dots) and closed loop (solid) conditions (each measured for 20 seconds). The circle represents the threshold related to the pointing requirement (2.1 μrad, rms). Figure 11 was measured with the structure driven over a broadband by a shaker mounted on the laboratory floor in order to excite rigid body motion. This data shows that the wavefront tilt control system regulates the angular error of the stellar beam well within the prescribed value when the instrument structure is disturbed (the closed loop data is essentially sensor noise). The same measurement for the other arm revealed the same result. Thus, the interference fringe detector is satisfied.

5. CONCLUSIONS

The control of wavefront tilt errors is a major contributor to the successful observation of interference fringes. Large feedback. should bc introduced to provide as much disturbance rejection as possible. The bandwidth of this control system is limited to 100 Hz by several factors. A 7th-order wavefront tilt control system was successfully implemented that provided 60 dB of feedback at low frequency while maintaining sufficient robustness to actuator saturation. Experimental verification of the control system's effectiveness in satisfying the interference fringe visibility requirement was obtained,

Although it is likely not necessary, the control system described in this paper could certainly bc improved. Increasing the order of the compensator to more carefully shape the loop gain is probably not the answer. This would quickly reach a point of diminishing returns, and would soon reduce the 100 Hz available bandwidth through calculation delay. The development of a Nyquist-stable control system would bc the next logical step in increasing the disturbance rejection capability of the wavefront tilt controller. With the constraint on loop gain roll-off steepness reduced (recall feedback limitation number 4 from section 4.2), the available feedback is increased. This would be feasible, however, only if a non-linear dynamic compensator was included in the design to ensure unconditional asymptotic global stability [5].

6. ACKNOWLEDGMENTS

The authors would like to thank the following individuals for their contribution to this work: Noble Nerhcim, Zahidul Rahman, Robert Laskin, and Boris Lurie at JPL, and John McInroy at the University of Wyoming. This research was performed at the Jet Propulsion Laboratory of the California Institute of Technology under contract with the National Aeronautics and Space Administration.

REFERENCES

[1] M.M. Colavita, M. Shao, M.D. Rayman, "0S1: Orbiting stellar interferometer for astrometry and imaging," Active Optics, Special Section of the Williamsburg Space Optics Conference, 1991.

[2 G.W. Neat, et al., "Micro-precision interferometer testbed: first stabilized stellar fringes," Procccdings of the SPIE International Symposium on AeroSense, Conference on Spaceborne Interferometry 11, vol. 2477, Orlando, FL, April 1995.

[3] B.E. Hines, "Optical design issues for the micro-precision interferometer testbed for space-based interferometry," Proceedings of the SPIE Symposium on OE/ Aerospace, Science and Sensing, Conference on Spaceborne Interferometry, vol. 1947, pp.44-57, Orlando, FL, April 1993.

[4 M.M. Colavita, "0S1 sensitivity, guide-star limiting magnitudes, and visibility reductions," JPL Interoffice Memorandum, Internal Document, Jet Propulsion Laboratory, California Institute of Technology, Pasadena, CA, March 1992.

[5] B.J. Luric, Feedback Maximization, Artcch House, Dedham, MA, 1986.